IEEE Open Journal of
Power Electronics

Received 16 May 2025; accepted 16 June 2025. Date of publication 26 June 2025;
date of current version 17 July 2025. The review of this article was arranged by Associate Editor Zhixiang Zou.

Digital Object Identifier 10.1109/OJPEL.2025.3583553

Estimation of Non-Stationary Frequency and Fundamental Components for Power Electronics-Dominated Energy Systems

PENG LI [1] (Member, IEEE), HIN SANG LAM [2] (Member, IEEE), BOLI CHEN [3] (Senior Member, IEEE), RAYMOND WAI M. NG [4] (Member, IEEE), THOMAS PARISINI [5,6,7] (Fellow, IEEE), AND S. Y. HUI [5,8] (Fellow, IEEE)

[1]School of Mechanical Engineering and Automation, Harbin Institute of Technology, Shenzhen 518000, China
[2]Department of Industrial and Systems Engineering, The Hong Kong Polytechnic University, Kowloon, Hong Kong
[3]Department of Electronic and Electrical Engineering, University College London, WC1E 6BT London, U.K.
[4]Department of Electrical and Electronic Engineering, The Hong Kong Polytechnic University, Hong Kong
[5]Department of Electrical and Electronic Engineering, Imperial College London, SW7 2AZ London, U.K.
[6]Department of Electronic Systems, Aalborg University, 9220 Aalborg, Denmark
[7]Department of Engineering and Architecture, University of Trieste, 34127 Trieste, Italy
[8]Department of Electrical Engineering, City University of Hong Kong, Kowloon Tong, Hong Kong

CORRESPONDING AUTHOR: S. Y. HUI (e-mail: eeronhui@cityu.edu.hk).

(Peng Li and Hin Sang Lam are co-first authors.)

This work was supported in part by the European Union's Horizon 2020 Research and Innovation Program under Grant 739551 (KIOS CoE), in part by the Italian Ministry for Research in the framework of the 2017 Program for Research Projects of National Interest (PRIN) under Grant 2017YKXYXJ, in part by the National Natural Science Foundation (NNSF) of China under Grant 62303133, in part by Shenzhen Fundamental Research Project JCYJ20220818102416036, and in part by City University of Hong Kong under Grant 9380173.

ABSTRACT Estimation of fundamental frequency and sinusoidal components is required for the regulation of modern power electronics-dominated power systems. Most of the existing estimation methods are designed for signals with *stationary* frequency. Hence, their accuracy could significantly degrade in the face of non-stationary frequencies, which is common in low-inertia power systems. In this paper, we propose a novel scheme for real-time estimation of a time-varying power frequency and the resulting fundamental signal. This is a time-domain method for (1) estimating *non-stationary* frequency and (2) fundamental signal reconstruction. It has the advantage of tracking the fundamental frequency component and treating all harmonics and subharmonics as noise. The method is based on a kernel-based estimation scheme and characterized by high accuracy, fast response, and noise immunity because of the inclusion of non-asymptotic kernel functions. The effectiveness of the proposed estimation scheme for non-stationary frequency tracking and fundamental signal reconstruction is verified by simulation and experimental results, which explore the use of the proposed scheme for frequency extraction of power signals appear in real world low-inertia systems.

INDEX TERMS Adaptive and nonlinear estimation, frequency detection, phase-locked loop, power component extraction.

NOMENCLATURE

s	Power signal affected by noise.
y_0, y_k	Fundamental and harmonic components.
c	DC current component.
y	Sum of DC current component and y_0.
y_f	Low pass filtered power signals.
ω, Ω	Fundamental frequency and its square.
A, θ	Amplitude and phase angle of y_0.
$K_h(t,\tau)$	Bivariate kernel functions, $h = 1, 2, 3$.
$K_h^{(i)}(t,\tau)$	ith order derivative of K_h with respect to τ.
κ, γ	Auxiliary signals.
t, s	Time and Laplace variable.
T_r	Resetting period.
$\sigma_1, \sigma_2, \sigma_3$	Pulse waves.
R_Ω, R_A	Residual signals.
$\dot{*}$, $\ddot{*}$, $\dddot{*}$	1st, 2nd, and 3rd time-derivatives of the signal.
sign$(*)$	Sigmoid function.

$\hat{*}$	Estimated signal.
$\lfloor * \rfloor$	Floor function, greatest integer less than or equal to $*$.
rem$(*)$	Remainder of the scalar division.

I. INTRODUCTION

The use of wind, solar, and other distributed energy resources in power generation is becoming increasingly important. These renewable energy sources are connected to distribution networks using power electronics devices, which can make controlling the power grid more challenging due to the lack of inertia. Maintaining global system stability, especially power system frequency stability, is a major challenge in modern power systems. This was evident during the recent blackout in Texas, where the system frequency dropped to 59.3 Hz [1].

With increasing amount of renewable energy sources connecting to power systems, power-electronics based devices are used as interfaces. Such nonlinear devices together with nonlinear loads tend to arouse harmonics/interharmonics in the overall system [2], [3]. Harmonic currents generated by these loads are transmitted back to the power distribution system through the point of common coupling (PCC), which causes harmonic voltages to appear and results in distortion at the PCC. Harmonics have several undesirable effects on the distribution system, including resistive losses, voltage stresses, overheating, and overloading of power components [4]. To address these issues, grid-connected converter control and compensator, e.g., Adaptive Power Filter (APF), are increasingly being used to mitigate harmonics in power lines [5], [6]. The control block of the APF involves a fast detection module to replicate the harmonic current for the power inverter to inject it into the power line. Therefore, fast and accurate estimation of the system frequency and power components is of paramount importance in power grid stability control.

Static state estimate that assumes the system frequency to be a constant (50 or 60 Hz), is used by the majority of power grid monitoring systems [7], [8]. The survey [9] provides a comprehensive review of commonly used estimation methods for APF applications including discrete Fourier transform (DFT), recursive DFT, synchronous fundamental dq-frame, and p-q theory. Additionally, recent modified DFT-based methods, as in [36], [37], [38], are proposed to deal with issue of the spectral leakage that enhance the estimation accuracy. It is noteworthy that DFT-based methods are suitable for single-phase applications whereas dq-frame and p-q methods can only be applied for three-phase systems. Additionally, Prony's method and its modifications (see [42], [43]) are also commonly used frequency estimation technique that provides high resolution and efficient parameter estimation but is sensitive to noise and requires careful handling of numerical stability and model order selection. The advantages and disadvantages of the frequency-domain methods such as DFT and time-domain methods such as Kalman filter, adaptive Notch filter etc. are addressed in [2].

Due to stochastic changes in demand and generation, power network frequencies are never operated in a steady-state condition in actual operation. The widespread integration of distributed renewable energy resources on the generating side and complicated loads with innovative demand-response technologies on the demand side, such as electric vehicles, makes this issue even worse. Due to the increased uncertainty caused by this shift in the system's dynamic properties, traditional estimation techniques based on the steady-state assumption of the fundamental frequency are unable to accurately monitor the modern power in a real-world setting.

In this context, dynamic state estimation (DSE) [10] with dynamic and uncertain frequency has become increasingly popular for time-critical monitoring, control, and protection of electric power grids resorting to widespread deployment of the phasor measurement units (PMUs), which provide basic measurement of synchrophasors, frequency, and rate of change of frequency (RoCoF) [11]. To achieve this, a range of DFT, least squares, and Kalman filtering techniques, and their variants have been quite successfully applied to DSE [12], [13], [14], [15], [16], [17], [18]. An unscented Kalman Filter is utilised for simultaneous estimation of the frequency and power components in [13]. In [16] interpolated DFT and Extended Kalman Filter are applied in series to estimate the RoCoF. The Phase-Locked-Loop (PLL) methods are still the most used approaches for estimating parameters of a sinusoidal power signal [19], [20], [21], [22], [23], [24], [25], [26]. More specifically, [19] proposes using the Taylor-Fourier filters in conjunction with the PLL to reduce the parameter estimation error of the PMU. PLLs that use quadrature signal generation (QSG) are commonly used for grid synchronization [21]. The Frequency Locked-Loop [22] uses a Second Order Generalized Integrator (SOGI) to implement the OSG and is capable of tracking sinusoidal signals with varying frequency and amplitude. Additional PLLs with frequency-adaptation ability can be found in [23] and [24]. Real-time monitoring and control of power system dynamics rely heavily on PMU accuracy. Therefore, there is a significant interest in improving PMU accuracy further.

In the spirit of prior work by the authors on the fundamental/harmonic component reconstruction with known and fixed fundamental frequency [2], an enhanced scheme is proposed to address the dynamic power signal estimation problem with time-varying and unknown fundamental frequency, which is essential for modern low-inertia power systems. The proposed solution method incorporates the main concepts of two recent estimation techniques: a kernel-based estimator [25] and a robust QPLL scheme [28]. In particular, the former is based on a suitably designed linear integral operator, which enables instantaneous sinusoidal parameter estimation for the case with a stationary frequency, while the latter represents a novel PLL architecture that has been proven to be more robust than existing solutions.

All in all, none of the above techniques are naturally designed for non-stationary frequency cases, thereby may not be able to provide reliable estimates (e.g., large latency, overshoot, etc.). This paper aims to fuse both techniques in [25] and [28] with suitable extensions so that the resulting scheme can cope with dynamic power signals. The key design involves a novel reinitializing mechanism, that periodically

resets the kernel-based algorithm to retain the fast convergence speed to parameter changes, a pre-filter for noise attenuation, and a post-compensation scheme to rectify the resulting phase lags and magnitude changes. Both simulation and experimental results are shown to verify the high accuracy and fast response of the proposed method in estimating fundamental frequency of signals in power electronics-dominated energy systems.

The paper is organized as follows. The dynamic estimation problem of the system frequency and main power component is formulated in Section II. Section III presents the main estimation algorithm is presented, and in Section IV, we provide numerical and experimental validation of the algorithm. Finally, Section V concludes the article with a discussion on future work.

II. PROBLEM STATEMENT AND PRELIMINARIES

A power signal can be represented by

$$s(t) = y(t) + n(t) \tag{1}$$

where $y(t)$ is the combination of the fundamental component $y_0(t) = A\sin\theta(t)$ and the dc component.

$$y(t) = c + A\sin\theta(t) \tag{2}$$

with amplitude A, angular frequency ω and initial phase θ_0, *i.e.* $\dot{\theta}(t) = \omega,\ \theta(0) = \theta_0$. c is the dc component and $n(t)$ represents the random noise, which subsumes higher order harmonics, measurement noise, etc. Note that the dc component is isolated from other disturbances $n(t)$ as complete removal of the dc component can be achieved by state-of-art estimators, such as augmented PLL [22]. Conversely, the unmodeled disturbances $n(t)$ are not specifically estimated due to the compromise between algorithm complexity and accuracy. Moreover, the high-order harmonics have small values comparing to the fundamental signal, therefore they are classified into noise for the first instance. Considering the practical scenario of power systems, we assume that the angular frequency ω is under slow variation within a small set encompassing the standard frequency, e.g., 50 Hz. The goal of this paper is to estimate the time-varying frequency $\omega(t)$ and the fundamental signal $y_0(t)$ with synchronized phase from the measurement $s(t)$.

In the rest of this section, we briefly review two recently proposed sinusoidal estimation methods since the concepts behind are instrumental for designing the proposed estimation scheme. For deeper insights on these approaches, readers are advised to refer to [25] and [28].

A. KERNEL-BASED FINITE-TIME ESTIMATION MECHANISM

A finite-time estimation scheme for parameter identification of $y(t)$ is proposed in [28] and [25] based on a typical linear integral operator, defined as

$$\left[V_K y\right](t) \triangleq \int_0^t K(t,\tau)\, y(\tau)\, d\tau,\ t \geq 0 \tag{3}$$

and the function $K(t,\tau)$ is a bivariate kernel function.

Three kernel functions are required in this task, and they are designed in the following form:

$$K_h(t,\tau) \triangleq e^{-\rho_h(t-\tau)}\left(1 - e^{-\bar{\rho}\tau}\right)^3,\ h = 1,2,3 \tag{4}$$

which is parametrized by user-defined coefficients $\rho_h > 0$ whereas $\bar{\rho} > 0$ is fixed for all three kernels. Denoting the ith partial derivative of the kernel with respect to τ by $K_h^{(i)}(t,\tau)$, the kernel is featured by $K_h^{(i)}(t,t) = 0,\ \forall\ i = 0,1,2$, which can be understood as the design criterion.

Considering $y(t)$ defined in (2), it is clear that the following equality holds:

$$\dddot{y}(t) = -\Omega\ \dot{y}(t) \tag{5}$$

where $\Omega = \omega^2$. Due to the linearity of the kernel operator (3), (5) further implies:

$$\left[V_{K_h}\dddot{y}\right](t) = -\Omega\left[V_{K_h}\dot{y}\right](t),\ h = 1,2,3. \tag{6}$$

where the image signals $[V_{K_h}\dddot{y}](t)$ and $[V_{K_h}\dot{y}](t)$ can be further expanded according to integral by parts as

$$\begin{aligned}\left[V_{K_h}\ddot{y}\right](t) = &\left[V_{K_h^{(3)}}y\right](t) - y(t)\,K_h^{(2)}(t,t)\\ &+ \dot{y}(t)\,K_h^{(1)}(t,t) - \ddot{y}(t)\,K_h(t,t)\end{aligned} \tag{7a}$$

$$\left[V_{K_h}y^{(1)}\right](t) = y(t)\,K_h(t,t) - \left[V_{K_h^{(1)}}y\right](t) \tag{7b}$$

As it can be noticed, the image signals $[V_{K_h^{(3)}}y](t)$ and $[V_{K_h^{(1)}}y](t)$ can be easily calculated by a linear system based on $y(t)$ as demonstrated in Appendix A. The only unknowns in (7) are $\dot{y}(t)$, $\ddot{y}(t)$. Hence, by solving the three equations in the form of (6) with respect to the three kernel functions, $\dot{y}(t)$, $\ddot{y}(t)$ can be canceled, yielding the linear regression model:

$$\kappa_1(t) = -\Omega\kappa_2(t) \tag{8}$$

where $\kappa_1(t)$ and $\kappa_2(t)$ depend only on *known* signals:

$$\begin{aligned}\kappa_1(t) = &\kappa_{a,1}\left(\kappa_{b,3} - \kappa_{b,2}\right) + \kappa_{a,2}\left(\kappa_{b,1} - \kappa_{b,3}\right)\\ &+ \kappa_{a,3}\left(\kappa_{b,2} - \kappa_{b,1}\right)\end{aligned} \tag{9a}$$

$$\begin{aligned}\kappa_2(t) = &\kappa_{d,1}\left(\kappa_{b,3} - \kappa_{b,2}\right) + \kappa_{d,2}\left(\kappa_{b,1} - \kappa_{b,3}\right)\\ &+ \kappa_{d,3}\left(\kappa_{b,2} - \kappa_{b,1}\right)\end{aligned} \tag{9b}$$

with

$$\kappa_{a,h}(\mathrm{t}) = \left[V_{K_h^{(3)}}y\right](t) - K_h^{(2)}(t,t)\,y(t), \tag{10a}$$

$$\kappa_{b,h}(\mathrm{t}) = K_{\mathrm{h}}^{(1)}(t,t),\ \kappa_{c,h}(t) = -K_h(t,t), \tag{10b}$$

$$\kappa_{d,h}(t) = \left[V_{K_h^{(1)}}y\right](t) - K_h(t,t)\,y(t),\ h = 1,2,3, \tag{10c}$$

As a result, the frequency estimation Ω can be obtained from the linear constraint (8). Various mathematical tools can be chosen to provide solutions to such a linear regressor model, such as recursive least square, gradient descent, etc. However, such methods rely on a continuous correction based

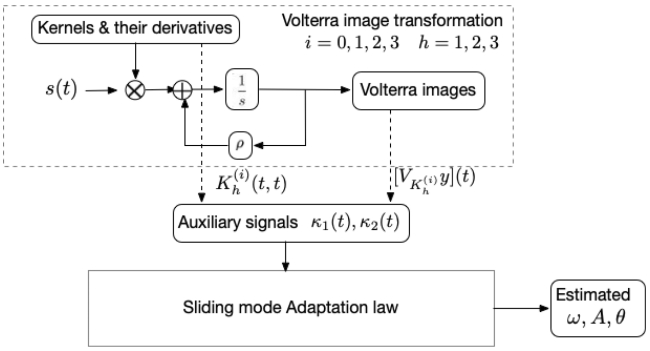

FIGURE 1. The flowchart of the kernel-based estimation scheme.

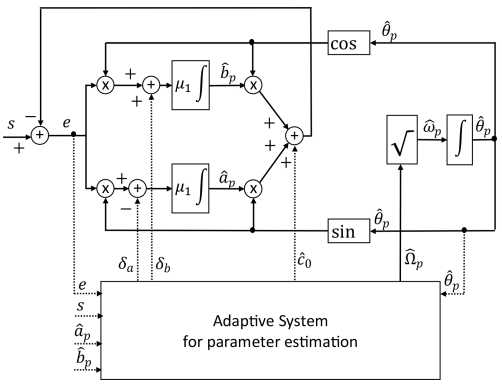

FIGURE 2. Scheme of the RGQPLL architecture. The dashed lines denote the additional signal paths compared to a conventional QSG-PLL.

on the error, therefore they tend to lengthen out the convergence time. On the other hand, direct algebraic solutions to (8) suffer from singularity issues. A specific example can be seen when $\kappa_2(t) = 0$, the estimator is not able to execute. Moreover, direct division in (8) to solve for Ω tends to be very sensitive to the measurement noise.

To circumvent this problem, an adaptive algorithm for estimating Ω, and in turn, estimating the fundamental signal $i_1(t)$, is proposed in [25]. This algorithm can identify parameters of a sinewave "almost instantaneously" (with finite-time convergence) as it is enabled. Based on the estimated frequency, the amplitude A and the instantaneous phase angle $\theta(t)$ can be further obtained in real-time. However, such fast convergence property cannot be preserved when a parameter change occurs during the operation.

A flowchart of the kernel-based estimator is depicted in Fig. 1.

B. ROBUST GLOBALLY CONVERGENT QPLL (RGQPLL)

The robust frequency-adaptive quadrature phase-locked-loop (RGQPLL) method is originally proposed in [28] to track the unknown frequency of sinusoidal signal $y(t)$. The architecture of RGQPLL is illustrated in Fig. 2. Compared to the conventional QSG-PLL, additional auxiliary signals (δ_a, δ_b, $\hat{c}_0(t)$, $\hat{c}_1(t)$) are generated and injected to the PLL scheme in addition to squared-frequency $\hat{\Omega}$, thereby robust global stability can be guaranteed [28].

The main algorithm is described by the following equations:

$$\dot{\hat{\Omega}}_p(t) = -k_0 y_1(t) e(t), \ \hat{\omega}_p(t) = \sqrt{\hat{\Omega}_p(t)} \tag{11a}$$

$$e(t) = s(t) - \hat{s}(t) \tag{11b}$$

$$\dot{\hat{\theta}}_p(t) = \sqrt{\Omega_p(t)} \tag{11c}$$

$$\dot{y}_1(t) = -\lambda_1 y_1 + s(t) \tag{11d}$$

$$\hat{s}(t) = \hat{a}_p(t) \sin\left(\hat{\theta}_p(t)\right) + \hat{b}_p(t) \cos\left(\hat{\theta}_p(t)\right) + \hat{c}_0(t) \tag{11e}$$

where the computation of auxiliary signals $\hat{a}_p(t), \hat{b}_p(t), \hat{c}_0(t)$ is given in Appendix B. k_0, λ_1 are positive design parameters. The tuning of the parameters is subject to the well-known tradeoff between convergence speed and steady state accuracy (noise sensitivity).

Both kernel-based and RGQPLL methods are designed for stationary sinusoidal signals that have constant frequencies. Injected by the non-stationary signals, the RGQPLL method tracks the signals with obvious latency due to asymptotic-converging transient. Moreover, the existence of high-order harmonics tends to further degrade the estimator performance. The kernel-based approach is featured with fast response; however, it is more vulnerable to noise $n(t)$ and the estimation error tends to accumulate as the fundamental frequency changes. In this paper, a new method is designed by integrating both methods with techniques of periodically resetting, filtering and compensation. The resulting method inherits the benefits of both methods with ability to fast track the time-varying frequency of non-stationary sinusoidal signals.

III. MAIN ESTIMATION ALGORITHM

In this section, our novel estimation scheme is introduced and designed for this specific application. The overall estimation scheme is composed of two steps. The first step is to extract the fundamental signal from the noisy measurement $s(t)$. The main principle of the fundamental signal estimator is based on the kernel-based parameter estimators introduced in Section II, but with a carefully designed periodical re-initialization mechanism, so that the fundamental signal with non-stationary frequency can be reconstructed. In the second step, with the reconstructed fundamental signal from the first step, an RGQPLL-based estimator is designed to track the time-varying frequency for further smoothing. The overall scheme of the proposed method is sketched in Fig. 3. It should be noted that this method can be applied to a single-phase system. Therefore, it is suitable for three-phase ones, too.

In the proposed scheme, the measurement $s(t)$ is first injected to a low-pass filter $F(s)$ to attenuate the disturbance. To cancel out the effects (e.g., amplitude scaling and phase lags) of the filter, a post-compensation mechanism is designed following the parameter estimators. Specifically, the filter signal

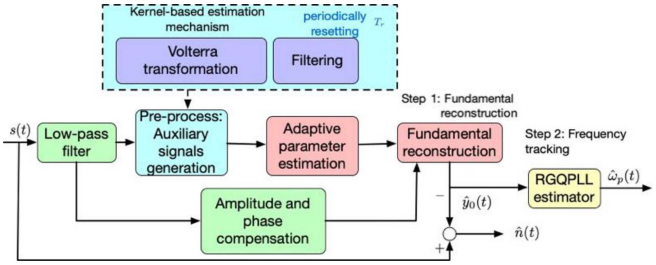

FIGURE 3. The flowchart of the proposed estimation scheme.

$s_f(t) = \mathcal{L}^{-1}\{F(s)\mathrm{s}(s)\}$ can be expressed as

$$s_f(t) = y_f(t) + n_f(t) \tag{12}$$

and

$$y_f(t) = c_f\,|F(0)| + |F(j\omega)|\,A\sin(\omega t + \varphi + \angle F(j\omega)), \tag{13}$$

where $|F(j\omega)|$ and $\angle F(j\omega)$ are the gain and phase angle of the filter $F(s)$ and $|F(0)|$. For the sake of brevity, let $A_f = |F(j\omega)|A$ and $\theta_f = \omega t + \varphi + \angle F(j\omega)$. Once the amplitude, frequency and phase (AFP) of $y_f(t)$ are available, the corresponding gain and phase shift brought by $F(s)$ can be easily calculated thus it is immediate to recover the fundamental signal $y(t)$ and the noise containing high-order harmonics $n(t)$.

According to (5) and recalling the linearity of $F(s)$, the filtered signal $y_f(t)$ verifies the differential equation:

$$\ddot{y}_f(t) = -\Omega\dot{y}_f(t). \tag{14}$$

Following the same line of reasoning as in [25], a fast-convergent sinusoidal estimator is designed in this paper along with a novel reinitializing scheme, which periodically resets the estimator every T_r seconds. The index of the resetting sequence is defined by $k = \lfloor \frac{t}{T_r} \rfloor$ and the remainder of the scalar division t/T_r is denoted by $\Delta T = \mathrm{rem}(t/T_r)$. As such, the integral defined in (3) is reinitialized with a period of T_r and correspondingly, the auxiliary signals in (9) and (10) are constructed based on the resetting mechanism by replacing t with ΔT in the kernel functions $K_h^{(i)}(t,\ t)\ \forall i, h = 0,\ 1,\ 2,\ 3$ and replacing $y(t)$ with $y_f(t)$. As a result, a new version of the linear regression model $\kappa_1(t) = -\Omega\kappa_2(t)$ is constructed for the signals calculated by the resetting mechanism. It is worth pointing out that the kernel function $K_h(\Delta T, \Delta T)$ and their derivatives $K_h^{(1)}(\Delta T, \Delta T), K_h^{(2)}(\Delta T, \Delta T), K_h^{(3)}(\Delta T, \Delta T)$ can be predetermined in an offline manner for the time interval $[0, T_r)$, which significantly saves online real-time computation power.

Following the same line of reasoning from (5) to (10), the linear constraint (8) can be obtained from the refined signals under the resetting mechanism. Owing to the positivity of the square frequency Ω, it follows that

$$|\kappa_1(t)| = -\Omega\,|\kappa_2(t)| \tag{15}$$

Now, let us introduce two auxiliary signals $\gamma_1(t)$ and $\gamma_2(t)$, the dynamics of which are governed by the following differential equations, driven by $|\kappa_1(t)|$ and $|\kappa_2(t)|$, respectively:

$$\dot{\gamma}_1(t) = |\kappa_1(t)| - \gamma_1(t), \tag{16a}$$

$$\dot{\gamma}_2(t) = |\kappa_2(t)| - \gamma_2(t), \tag{16b}$$

$$\gamma_1(t) = \gamma_2(t) = 0, \text{ if } \Delta T = 0.$$

It can be inferred from (15) and (16) that $\gamma_1(t) = -\Omega\gamma_2(t)$, from which many methods can be used to develop an adaptive estimation law, e.g., gradient descent, least squares. In this work, a sliding-mode-based adaptive frequency estimator is devised for fast convergence speed, exploiting the residual signal $R_\Omega = \gamma_1(t) + \gamma_2(t)\hat{\Omega}(t)$ (that is non-zero unless $\hat{\Omega}(t) = \Omega$):

$$\dot{\hat{\Omega}}(t) = \gamma_2(t)^{-1}\Big(\eta_\Omega(t) + L_1\sqrt{|R_\Omega|}\mathrm{sign}(R_\Omega(t)) - \hat{\Omega}(t)\dot{\gamma}_2(t) + \dot{\gamma}_1(t)\Big)\,\sigma_1(\Delta T), \tag{17a}$$

$$\dot{\eta}_\Omega(t) = L_2\mathrm{sign}(R_\Omega(t))\,\sigma_1(\Delta T), \tag{17b}$$

where the initial guess $\hat{\Omega}(0)$ can be set to the square of the nominal frequency (i.e., 100π rad/s). $\sigma_1(\Delta T)$ is a pulse wave that determines the on/off switching of the adaptation (see Fig. 6 for a specific example). In each cycle, the pulse wave starts from value 0 with the rising edge occurs at $\Delta T = T_{c,1}(i.e.,\ t = kT_r + T_{c,1})$. $T_{c,1}$ is a small constant by which $\sigma_1(\Delta T) = 0$ during the time interval $[kT_r, kT_r + T_{c,1})$. Thus, $\hat{\Omega}(t)$ remains constant at $\hat{\Omega}(kT_r^-)$, where kT_r^- is the time instant before kT_r. As such, the numerical issue due to $\gamma_2(kT_r) = 0$ (not invertible) is prevented by design.

Resorting to the squared frequency estimate $\hat{\Omega}(t)$ and (10), the real-time estimates of $\dot{y}_f(t)$ and $\ddot{y}_f(t)$ are available, as shown in (18) at the bottom of the next page. As it can be noticed, the estimates of $\dot{y}_f(t)$ and $\ddot{y}_f(t)$ are not available at the resetting instants as the denominator of both expressions is 0 when $\Delta T = 0$. Analogously to the frequency estimation, another pulse wave, $\sigma_2(\Delta T)$ is utilized (see Fig. 6 for a specialized example), which disables the nominal estimation scheme (18) for $t \in [kT_r, kT_r + T_{c,2})$ with $T_{c,2}$ a small time instant defining the rising edge of $\sigma_2(\Delta T)$. Instead, the estimates at $t = kT_r^-$ are maintained during this interval, leading to

$$\widehat{\dot{y}}_f(t) = \widehat{\dot{y}}_f^*(t)\,\sigma_2(\Delta T) + \widehat{\dot{y}}_f(kT_r)(1 - \sigma_2(\Delta T)) \tag{19a}$$

$$\widehat{\ddot{y}}_f(t) = \widehat{\ddot{y}}_f^*(t)\,\sigma_2(\Delta T) + \widehat{\ddot{y}}_f(kT_r)(1 - \sigma_2(\Delta T)) \tag{19b}$$

Consider the structural constraint:

$$\Omega\dot{y}_f(t)^2 + \ddot{y}_f(t)^2 = A_f^2\Omega^2. \tag{20}$$

The amplitude of the fundamental signal is estimated analogously to the frequency estimation algorithm (17) by employing the residual

$$R_A(t) \triangleq \gamma_3 - \hat{A}_f(t)\,\gamma_4(t),$$

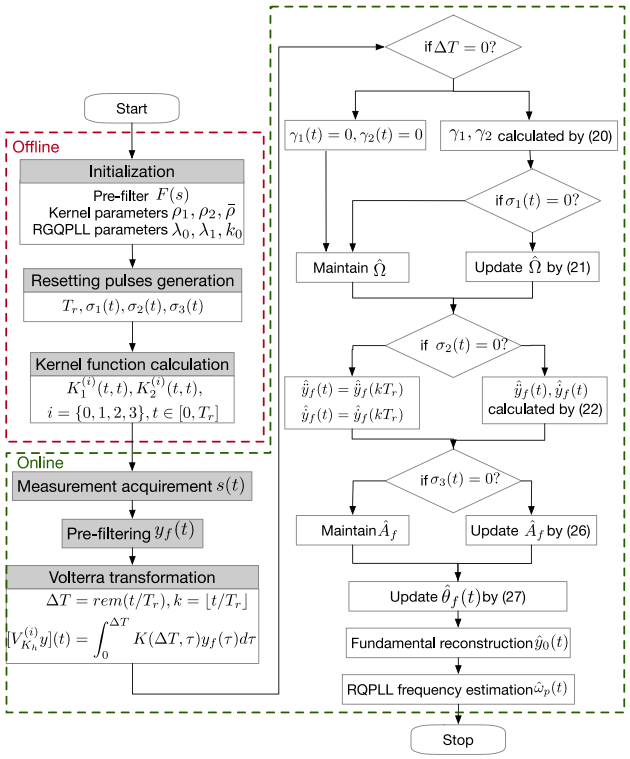

FIGURE 4. Flowchart of the algorithm.

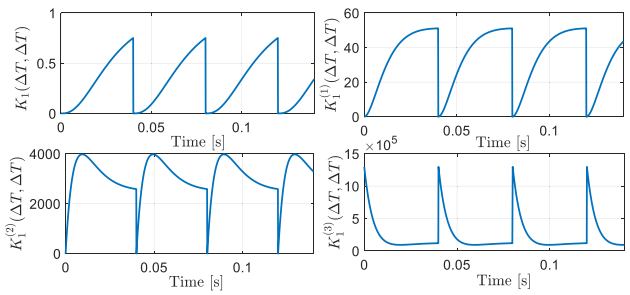

FIGURE 5. The reinitialized kernels $K_1^{(i)}(\Delta T, \Delta T)$, $i = \{0, 1, 2, 3\}$.

where γ_3 and γ_4 are the filtered signals, obtained by

$$\dot{\gamma}_3(t) = \left| \sqrt{\hat{\Omega}(t) \hat{\ddot{y}}_f(t)(t)^2 + \hat{\dot{y}}_f(t)(t)^2} \right| - \gamma_3, \tag{21a}$$

$$\dot{\gamma}_4(t) = \left| \hat{\Omega}(t) \right| - \gamma_4(t), \tag{21b}$$

$$\gamma_3(t) = \gamma_4(t) = 0, if\ \Delta T = 0$$

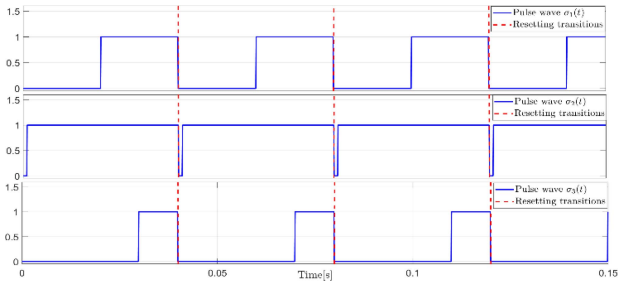

FIGURE 6. Periodic pulse waves embedded in the parameter adaptation scheme.

Thus, the amplitude estimates are accomplished by

$$\dot{\hat{A}}_f(t) = \gamma_3(t)^{-1} \left(\eta_A(t) + \sqrt{|R_A|} \text{sign}(R_A(t)) - \hat{A}(t) \dot{\gamma}_3(t) + \dot{\gamma}_4(t) \right) \sigma_3(\Delta T) \tag{22a}$$

$$\dot{\eta}_A(t) = \text{sign}(R_A(t)) \sigma_3(\Delta T) \tag{22b}$$

where $\hat{A}_f(0) = \eta_A(t) = 0$ and $\sigma_3(\Delta T)$ is another pulse wave, like $\sigma_1(\Delta T)$ and $\sigma_2(\Delta T)$ (see Fig. 6 for a specific example). However, the transition from 0 to 1 occurs at $\Delta T = T_{c,3} > \max(T_{c,1}, T_{c,2})$ as the amplitude estimation relies on the estimates $\hat{\Omega}(t)$, $\hat{\dot{y}}_f(t)$ and $\hat{\ddot{y}}_f(t)$.

Finally, the phase is estimated by

$$\hat{\theta}_f(t) = \angle \left[\hat{\omega}_k(t) \hat{\dot{y}}_f(t) - j \hat{\ddot{y}}_f(t) \right] + 100\pi \Delta T (1 - \sigma_2(\Delta T)) \tag{23}$$

where j denotes the complex imaginary unit and the frequency estimate $\hat{\omega}_k(t)$ is directly obtained by $\hat{\omega}_k(t) = \sqrt{\hat{\Omega}(t)}$. It is worth noting that the first term of (23) is based on the standard formula for the angular phase evaluation, which is constant during the short time interval $t \in [kT_r, kT_r + T_{c,2})$ as $\hat{\dot{y}}_f(t)$ and $\hat{\ddot{y}}_f(t)$ are frozen. A simple correction scheme is appended by assuming that the instantaneous frequency is 50 Hz. Being the actual frequency of the line current within a small range around 50 Hz (i.e., [45 Hz, 55 Hz]), the proposed compensation mechanism can achieve very satisfactory accuracy (as will be shown later by simulation and experimental tests). Finally, the nominal fundamental signal can be reconstructed by compensating the gain and phase shifts of the low-pass filter $F(s)$: the fundamental component is obtained by

$$\hat{y}_0(t) = \frac{\hat{A}_f(t)}{|F(j\hat{\omega})|} \sin\left(\hat{\theta}_f(t) - \angle F(j\hat{\omega}) \right), \tag{24}$$

$$\hat{\dot{y}}_f^*(t) = \frac{K_1(\Delta T, \Delta T)\left(\kappa_{a,2}(t) + \hat{\Omega}(t)\kappa_{d,2}(t)\right) - K_2(\Delta T, \Delta T)\left(\kappa_{a,1}(t) + \hat{\Omega}(t)\kappa_{d,1}(t)\right)}{K_1^{(1)}(\Delta T, \Delta T) K_2(\Delta T, \Delta T) - K_1(\Delta T, \Delta T) K_2^{(1)}(\Delta T, \Delta T)} \tag{18a}$$

$$\hat{\ddot{y}}_f^*(t) = \frac{K_1^{(1)}(\Delta T, \Delta T)\left(\kappa_{a,2}(t) + \hat{\Omega}(t)\kappa_{d,2}(t)\right) - K_2^{(1)}(\Delta T, \Delta T)\left(\kappa_{a,1}(t) + \hat{\Omega}(t)\kappa_{d,1}(t)\right)}{K_1^{(1)}(\Delta T, \Delta T) K_2(\Delta T, \Delta T) - K_1(\Delta T, \Delta T) K_2^{(1)}(\Delta T, \Delta T)} \tag{18b}$$

where $|F(j\hat{\omega})|$ and $\angle F(j\hat{\omega})$ are the gain and phase angle of the filter $F(s)$ at estimated frequency $\hat{\omega}$.

To achieve a smooth frequency estimate to facilitate frequency-based diagnosis, control, etc., the reconstructed fundamental signal is injected to the RGQPLL frequency estimator, introduced in Section II-B. To be specific, replacing $s(t)$ in (11) with the estimated fundamental signal $\hat{y}_0(t)$ obtained in (24), the frequency estimate $\hat{\omega}_p(t)$ can be obtained in real-time.

IV. NUMERICAL AND EXPERIMENTAL VALIDATION

In this section, the effectiveness of the proposed scheme is verified by both numerical and experimental tests of the power systems. A flowchart is given in Fig. 4 which illustrates the process of algorithm implementation.

A. INITIALIZATION OF THE ALGORITHM

The parameter choices are given in this subsection, including the design of the prefilter, and coefficients of the kernel functions, resetting periods and RGQPLL parameters.

Pre-filter: The low-pass filter $F(s)$ is designed as second-order Butterworth filter for a compromise between response speed and computational complexity:

$$F(s) = \frac{\omega_c^2}{s^2 + 1.4142\,\omega_c s + \omega_c^2}$$

where the cutting off frequency is $\omega_c = 120\pi$ rad/s. As such, the high-order harmonics can be attenuated whereas the fundamental signal is retained.

Given a frequency estimate $\hat{\omega}(t)$, the gain and the phase angle of $F(s)$ can be computed as follows:

$$|F(j\hat{\omega})| = \frac{\omega_c^2\sqrt{\omega_c^4 + \hat{\omega}^4(t)}}{\omega_c^4 + \hat{\omega}^4(t)},$$

$$\angle F(j\hat{\omega}) = \tan^{-1}\left[\frac{1.4142\omega_c\hat{\omega}(t)}{\omega_c^2 - \hat{\omega}^2(t)}\right].$$

Kernel-based estimator: The kernel functions are designed by choosing: $\rho_1 = 50$, $\rho_2 = 80$, $\rho_3 = 100$, $\bar{\rho} = 60$, such that the kernels employed for evaluation of auxiliary signal $\kappa_1(t)$, $\kappa_2(t)$ and the transformed signals $[V_{K_h^{(1)}}y](t)$, $[V_{K_h^{(3)}}y](t)$ are given in (25) at the bottom of the next page. In addition, the waveforms of $K_1^{(i)}(\Delta T, \Delta T)$, $i =$

$$\begin{bmatrix} K_1(\Delta T,\ \Delta T) \\ K_1^{(1)}(\Delta T,\ \Delta T) \\ K_1^{(2)}(\Delta T,\ \Delta T) \\ K_1^{(3)}(\Delta T,\ \Delta T) \end{bmatrix} =$$

$$\begin{bmatrix} \left(1 - e^{-60\Delta T}\right)^3 \\ 180e^{-60\Delta T}\left(e^{-60\Delta T} - 1\right)^2 - 50\left(e^{-60\Delta T} - 1\right)^3 \\ 7200e^{-60\Delta T}\left(e^{-60\Delta T} - 1\right)^2 - 21600e^{-120\Delta T}\left(e^{-60\Delta T} - 1\right) - 2500\left(e^{-60\Delta T} - 1\right)^3 \\ 1296000e^{-180\Delta T} + 648000e^{-120\Delta T}\left(e^{-60\Delta T} - 1\right) + 378000e^{-60\Delta T}\left(e^{-60\Delta T} - 1\right)^2 - 125000\left(e^{-60\Delta T} - 1\right)^3 \end{bmatrix}$$

$$\begin{bmatrix} K_2(\Delta T,\ \Delta T) \\ K_2^{(1)}(\Delta T,\ \Delta T) \\ K_2^{(2)}(\Delta T,\ \Delta T) \\ K_2^{(3)}(\Delta T,\ \Delta T) \end{bmatrix} =$$

$$\begin{bmatrix} \left(1 - e^{-60\Delta T}\right)^3 \\ 180e^{-60\Delta T}\left(e^{-60\Delta T} - 1\right)^2 - 80\left(e^{-60\Delta T} - 1\right)^3 \\ 18000e^{-60\Delta T}\left(e^{-60\Delta T} - 1\right)^2 - 21600e^{-120\Delta T}\left(e^{-60\Delta T} - 1\right) - 6400\left(e^{-60\Delta T} - 1\right)^3 \\ 1296000e^{-180\Delta T} - 1296000e^{-120\Delta T}\left(e^{-60\Delta T} - 1\right) + 1512000e^{-60\Delta T}\left(e^{-60\Delta T} - 1\right)^2 - 512000\left(e^{-60\Delta T} - 1\right)^3 \end{bmatrix} \quad (25)$$

$$\begin{bmatrix} K_3(\Delta T,\ \Delta T) \\ K_3^{(1)}(\Delta T,\ \Delta T) \\ K_3^{(2)}(\Delta T,\ \Delta T) \\ K_3^{(3)}(\Delta T,\ \Delta T) \end{bmatrix} =$$

$$\begin{bmatrix} \left(1 - e^{-60\Delta T}\right)^3 \\ 180e^{-60\Delta T}\left(e^{-60\Delta T} - 1\right)^2 - 100\left(e^{-60\Delta T} - 1\right)^3 \\ 252000e^{-60\Delta T}\left(e^{-60\Delta T} - 1\right)^2 - 21600e^{-120\Delta T}\left(e^{-60\Delta T} - 1\right) - 10000\left(e^{-60\Delta T} - 1\right)^3 \\ 1296000e^{-180\Delta T} - 2592000e^{-120\Delta T}\left(e^{-60\Delta T} - 1\right) + 2808000e^{-60\Delta T}\left(e^{-60\Delta T} - 1\right)^2 - 1000000\left(e^{-60\Delta T} - 1\right)^3 \end{bmatrix}$$

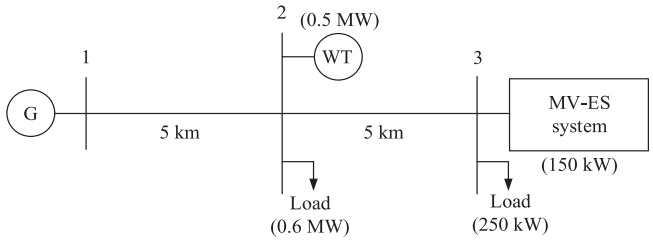

FIGURE 7. Diagram of the three-bus ac microgrid.

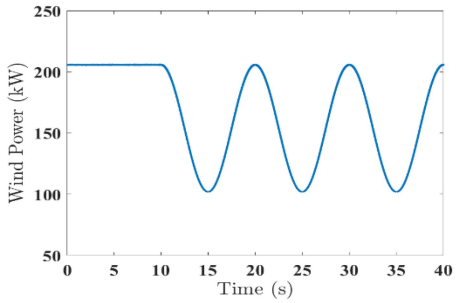

FIGURE 8. The wind profile for the medium voltage electric spring simulation.

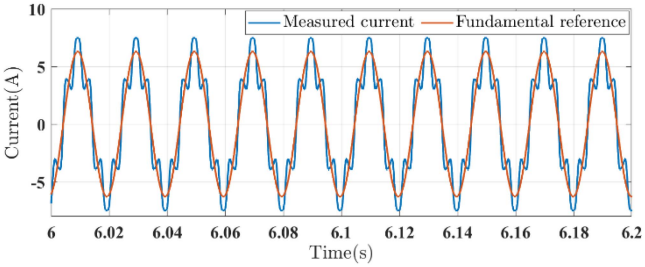

FIGURE 9. Current measurement containing the harmonics.

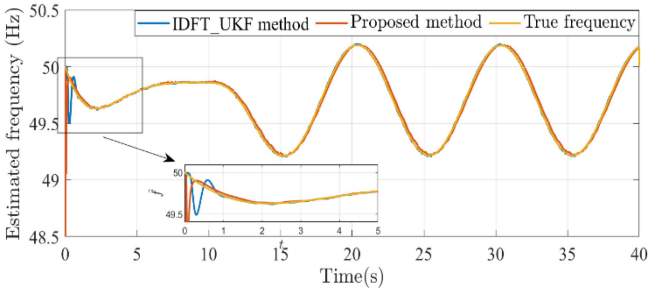

FIGURE 10. Frequency estimation results.

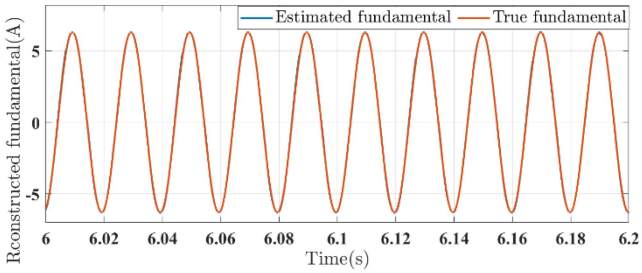

FIGURE 11. Fundamental current estimation results.

{0, 1, 2, 3} (with reinitialization) are shown in Fig. 5 as illustrative examples. The pulse signals σ_1, σ_2, σ_3 are designed by choosing $T_{c,1}$= 20ms, $T_{c,2}$ = 1ms, $T_{c,3}$ = 30ms. Thereby the resulting waveforms are shown in Fig. 6, where the overall resetting sequences are highlighted. Finally, the overall resetting period, T_r is set to 40 ms which amounts to two cycles of the fundamental signal so as to ensure sufficient sensitivity to a parameter change.

RGQPLL: The tuning parameters of the RGQPLL method are chosen as $\lambda_0 = 800$, $\lambda_1 = 600$, $k_0 = 1 \times 10^8$.

B. POWER SYSTEM SIMULATION

A modified test case of the power system with reference to [32], [33], [34] is considered herein, showing the effectiveness of the proposed scheme dealing with fundamental signal identification and frequency tracking in real systems. In practical applications, fast frequency and fundamental estimation are especially crucial for grid-connected compensators and converter control, to stabilize the power system with large-scale renewable energy integration.

In this numerical test, a 6.6-kV three-bus ac microgrid as shown in Fig. 7 is considered, which consists of a generator G on Bus 1, a wind turbine (WT) and a resistive load on Bus 2, and a modular multilevel cascade converter (MMCC)-fed battery load and a non-linear load on Bus 3. There are two 5-km distribution lines between Bus 1 and 2 and between Bus 2 and 3. The wire resistance and inductance of the distribution line are 0.237Ω/km and 1.064 mH/km, respectively [35]. The initial power of each element is also marked in the figure. A wind-profile as shown in Fig. 8 has been used to fluctuate the output power between 100 and 200 kW for a period of 10s, which results in a continuously changing frequency variation (see Fig. 10). Notably, a nonlinear load is connected therefore introducing high order harmonics in the current measurement. The harmonic content is referenced to [9], as shown in Fig. 9.

Injecting the afore-shown current measurement to the proposed estimation scheme, the grid frequency variation and the fundamental component of the current are identified as depicted in Figs. 10 and 11. Moreover, the proposed method is compared with an IDFT-UKF method recently proposed in [16] which is also featured by the fast-tracking response. As fundamental estimation is not involved in [16], a comparison of only frequency estimation is presented herein.

As can be noticed from Fig. 10, both methods are able to provide frequency tracking. However, thanks to the non-asymptotic feature of the kernel-based estimation, the proposed estimation scheme shows a faster convergence speed in the initial phase. On the other hand, Fig. 11 confirms the fact

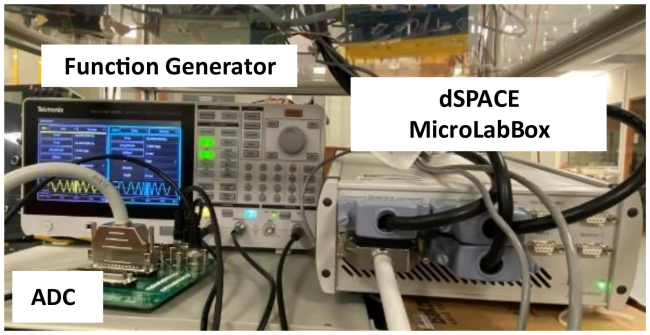

FIGURE 12. The experimental setup.

TABLE 1 Fundamental and Harmonic Content to Reference Waveform [30]

Fundamental/Harmonic	Voltage (V)
dc offset	0
Fundamental	7.8
5th harmonic	2.25
7th harmonic	0.39
11th harmonic	0.39
13th harmonic	0.39

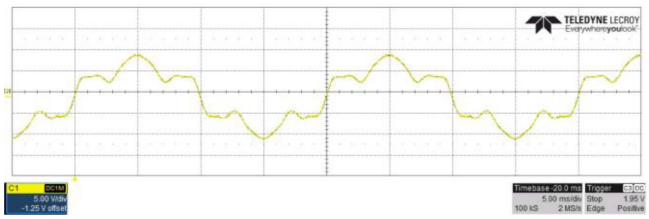

FIGURE 13. The power signal corrupted by harmonics.

that the fundamental current component is reconstructed from the harmonic-contaminated measurement without amplitude change and phase shift which are commonly seen in typical filtering techniques. In addition, the proposed method can provide real-time fundamental reconstruction that turns out to be instrumental for grid-connected compensators, such as active power filters.

C. EXPERIMENTAL TEST

Practical tests as shown in Fig. 12 have been conducted to evaluate the reconstructed fundamental and frequency tracking performance of kernel-based method. The harmonic content of the reference waveform used in this test is tabulated in Table 1, and the waveform is illustrated in Fig. 13. The reference waveform is based on the example (with the same relative harmonic ratios) used in the comparison in [30] for a range of harmonic detection methods. Three cases of RoCoF (0.2 Hz/s, 0.4 Hz/s and 1 Hz/s) from 48-52 Hz have been selected to study based on [31]. The reset time is $T_r = 0.04$s and the sampling frequency is 10 kHz. The harmonic signal is programmed on the function generator Tektronix AFG31000

TABLE 2 Error of The Estimated Frequency

RoCoF (Hz/s)	RMS error (Hz)	Maximum error (Hz)
0.2	0.0294	0.0653
0.4	0.0481	0.0891
1	0.1026	0.1653

TABLE 3 Error of The Reconstructed Fundamental

RoCoF (Hz/s)	RMS error (V)	Error range (V)
0.2	0.2798	1.9625
0.4	0.2795	1.9016
1	0.2803	1.8145

and the algorithm is implemented by dSPACE microlabbox. Before carrying out the experiment, the steady-state signal is sampled and processed by the algorithm to eliminate the error from convergence.

The following method has been used to calculate the error which eliminates the phase error between the reconstructed fundamental and reference fundamental. Firstly, a pre-designed waveform as shown in Fig. 13 is injected by a functional generator to the dSPACE. Also, a fundamental waveform is injected to the dSPACE at the same time. Hence, the reconstructed fundamental waveform will be subtracted by the injected fundamental waveform in the program and further analysis can be carried out by capturing the data. The method minimized the phase error between the reconstructed and injected fundamental as the functional generator provides the two signals that are perfectly in phase.

Table 2 shows the RMS error and the maximum error of the estimated frequency. Table 3 shows the RMS error and the error range of the reconstructed fundamental. The RMS error and error range have no significant change under different RoCoF. It shows that the algorithm can work in a wide range of frequency and provide an excellent reconstructed fundamental.

Fig. 14(a) to (c) show the actual and estimated frequency by the proposed method. These results again confirm the algorithm can operate under a wide range of frequency. Fig. 15(a) to (c) show 10 cycles of the reconstructed fundamental with the reference fundamental. The two time-behaviors are almost the same and overlap with each other. The three figures do not have any observable difference or distortion with the increase of the frequency. This set of results matches the error calculation in Table 3 and again confirms that the algorithm can operate in a wide range of frequency with excellent reconstructed fundamental and frequency tracking performance.

V. CONCLUDING REMARKS

Based on the algorithms [25], [28] previously developed for ***stationary*** signals, a novel time-domain frequency estimation scheme is developed and proposed for real-time estimation of ***non-stationary*** power signals. The method has the distinct

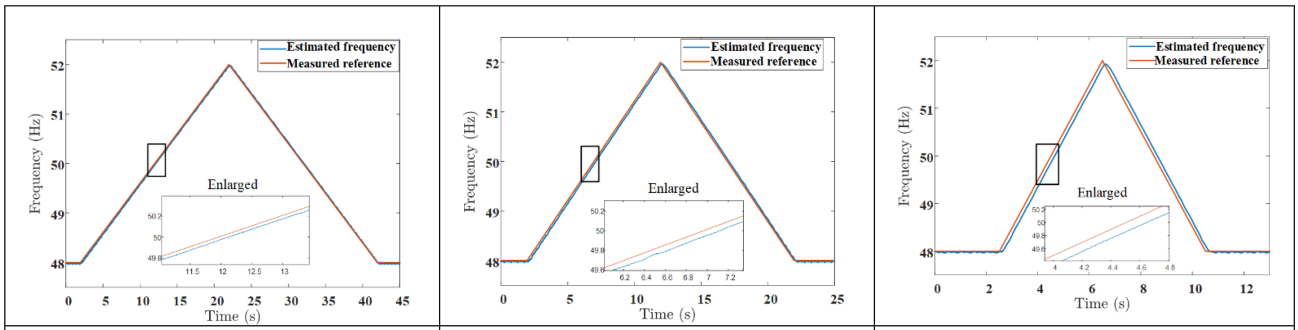

(a) Frequency estimation with RoCoF 0.2Hz/s | (b) Frequency estimation with RoCoF 0.4Hz/s | (c) Frequency estimation with RoCoF 1Hz/s

FIGURE 14. (a) Frequency estimation with RoCoF 0.2 Hz/s. (b) Frequency estimation with RoCoF 0.4 Hz/s. (c) Frequency estimation with RoCoF 1 Hz/s.

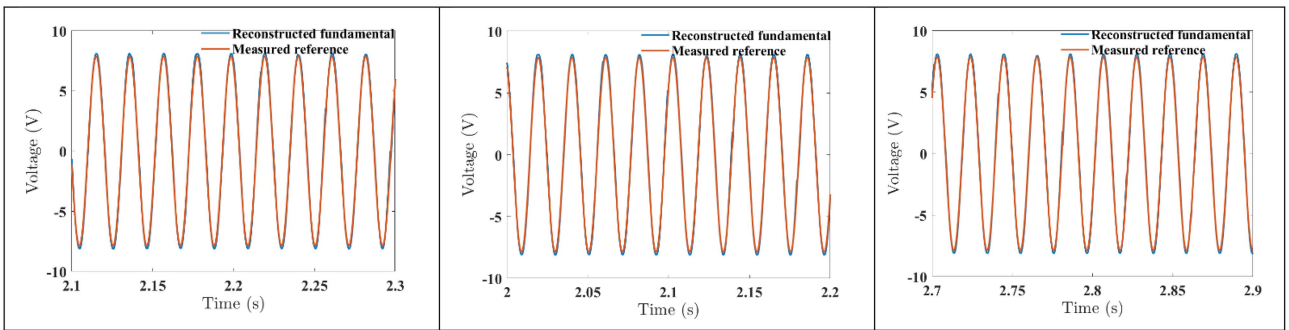

(a) Reconstructed fundamental with RoCoF 0.2 Hz/s | (b) Reconstructed fundamental with RoCoF 0.4 Hz/s | (c) Reconstructed fundamental with RoCoF 1Hz/s

FIGURE 15. (a) Reconstructed fundamental with RoCoF 0.2 Hz/s. (b) Reconstructed fundamental with RoCoF 0.4 Hz/s. (c) Reconstructed fundamental with RoCoF 1 Hz/s.

advantage of achieving both fundamental reconstruction and frequency tracking. Deploying suitably designed filtering and integral operators, the effects of the harmonics and noise can be annihilated. Therefore, this method is robust against complete orders of harmonics, subharmonics and interharmonics in the power grid. The novel resetting mechanism eliminates the error accumulation in typical static state estimation, so that the fundamental signal can be reconstructed almost instantaneously. Consequently, the time-varying frequency of the signal can be identified smoothly. The proposed method is not computationally intensive and can be implemented in the processor with a sampling frequency of only several kilo-Hertz. It can be applied for monitoring frequency variations in weak power grids and power-electronics-dominated power grids. Both numerical and experimental tests are conducted reproducing practical circumstances in real-world power systems. The practical results show that the proposed estimation method can provide fast and accurate fundamental and frequency.

APPENDIX A

In the proposed estimation scheme, $[V_{K_h^{(1)}}y](t)$ and $[V_{K_h^{(3)}}y](t)$ are the Volterra images that are involved in the estimator as in (10), $\forall h = 1, 2, 3$. Defining the vector of the Volterra image vector:

$$\xi(t) = \left[\xi_1(t)^\top, \xi_2(t)^\top, \xi_3(t)^\top\right]^\top$$

with

$$\xi_h(t) = \left[\left[V_{K_h^{(1)}}y\right](t), \left[V_{K_h^{(3)}}y\right](t)\right]^\top, \quad h = 1, 2, 3,$$

it holds that $\dot{\xi}(t) = -G\xi(t) + E(t)y(t)$, with $\xi(0) = 0$ and

$$G = \text{diag}\left(\rho_1, \rho_1, \rho_2, \rho_2, \rho_3, \rho_3\right),$$

$$E(t) = \left[E_1(t)^\top, E_2(t)^\top, E_3(t)^\top\right]^\top$$

with $E_h(t) = [K_h^{(1)}(t,t), K_h^{(3)}(t,t)]^\top$, $h = 1, 2, 3$.

APPENDIX B

The auxiliary signals $\hat{a}_p(t), \hat{b}_p(t), \hat{c}_0(t)$ of the RGQPLL scheme are calculated by

$$\dot{\hat{a}}_p(t) = (\lambda_0 + \lambda_1)\sin\left(\hat{\theta}_p\right)e(t) - \delta_a(t),$$

$$\dot{\hat{b}}_p(t) = (\lambda_0 + \lambda_1)\cos\left(\hat{\theta}_p\right)e(t) + \delta_b$$

$$\dot{\hat{c}}_0(t) = \hat{c}_1(t) + \sqrt{\Omega_p(t)}\left(\hat{b}_p(t)\sin(\hat{\theta}_p) - \hat{a}_p(t)\cos\left(\hat{\theta}_p\right)\right)$$

$$\dot{\hat{c}}_1(t) = \left(\lambda_0\lambda_1 - \hat{\Omega}_p(t)\right) e(t) - \hat{\Omega}_p(t)\ \hat{y}(t) + \hat{K}(t) - y_1(t)\,\hat{\Omega}_p(t) + \frac{1}{\lambda_1} k_0 e(t),$$

$$\eta_0(t) = 1 - \frac{\mu_0}{\hat{\Omega}_{\mathrm{p}}(t)},\ \eta_1(t) = -\frac{\mu_1}{\hat{\Omega}_{\mathrm{p}}(t)} - \frac{\dot{\hat{\Omega}}_p(t)}{2\hat{\Omega}_p^2(t)},$$

$$\delta_a = \sqrt{\Omega_p(t)}\cos\left(\hat{\theta}_p\right)\left(\eta_0(t)\,\hat{c}_0(t) + \eta_1(t) \times \left(c_1(t) + \sqrt{\Omega_p(t)}\left(\hat{b}(t)\sin\left(\hat{\theta}_p\right) - \hat{a}_p(t)\cos(\hat{\theta}_p)\right)\right)\right),$$

$$\delta_b = \sqrt{\Omega_p(t)}\sin(\hat{\theta}_p)(\eta_0(t)\hat{c}_0(t) + \eta_1(t)(c_1(t) + \sqrt{\Omega_p(t)}(\hat{b}(t)\sin(\hat{\theta}_p) - \hat{a}_p(t)\cos(\hat{\theta}_p))).$$

where $\lambda_0 > 0$ is the third design parameter in addition to k_0 and λ_1.

REFERENCES

[1] U.S. House of Representatives, *Comm. Energy Commerce, Subcomm. Oversight Investigations, Climate Change: The Impacts of the Atlantic Coast Pipeline*, Hearing HHRG-117-IF02-20210324-SD007. [Online]. Available: https://docs.house.gov/meetings/IF/IF02/20210324/111365/HHRG-117-IF02-20210324-SD007.pdf

[2] B. Chen, G. Pin, W. M. Ng, T. Parisini, and S.-Y. R. Hui, "A fast-convergent modulation integral observer for online detection of the fundamental and harmonics in grid-connected power electronics systems," *IEEE Trans. Power Electron.*, vol. 32, no. 4, pp. 2596–2607, Apr. 2017.

[3] B. Chen, G. Pin, W. M. Ng, P. Li, T. Parisini, and S.-Y. R. Hui, "Online detection of fundamental and interharmonics in AC mains for parallel operation of multiple grid-connected power converters," *IEEE Trans Power Electron.*, vol. 33, no. 11, pp. 9318–9330, Nov. 2018.

[4] K. Patil and W. Gandhare, "Effects of harmonics in distribution systems on temperature rise and life of XLPE power cables," in *Proc. Int. Conf. Power Energy Syst.*, 2011, pp. 1–6.

[5] H. Akagi, "New trends in active filters for power conditioning," *IEEE Trans. Ind. Appl.*, vol. 32, no. 6, pp. 1312–1322, Nov./Dec. 1996.

[6] H. Akagi, "Active harmonic filters," *Proc. IEEE*, vol. 93, no. 12, pp. 2128–2141, Dec. 2005.

[7] A. Abur and A. Gomez-Expósito, *Power System State Estimation: Theory and Applications*. Boca Raton, FL, USA: CRC Press, 2004.

[8] B. P. McGrath, D. G. Holmes, and J. J. H. Galloway, "Power converter line synchronization using a discrete fourier transform (DFT) based on a variable sample rate," *IEEE Trans. Power Electron.*, vol. 20, no. 4, pp. 877–884, Jul. 2005.

[9] L. Asiminoaei, F. Blaabjerg, and S. Hansen, "Evaluation of harmonic detection methods for active power filter applications," in *Proc. IEEE 20th Annu. Appl. Power Electron. Conf. Expo.*, 2005, pp. 635–641.

[10] A. Abur, "Dynamic-state estimation," in *Smart Grid Handbook*. Chichester, U.K.: Wiley, 2016, pp. 1–14.

[11] A. G. Phadke and J. S. Thorp, *Synchronized Phasor Measurements and Their Applications*. New York, NY, USA: Springer-Verlag, 2008.

[12] E. Ghahremani and I. Kamwa, "Online State estimation of a synchronous generator using unscented Kalman filter from phasor measurements units," *IEEE Trans. Energy Convers.*, vol. 26, no. 4, pp. 1099–1108, Dec. 2011.

[13] P. Regulski and V. Terzija, "Estimation of frequency and fundamental power components using an unscented Kalman filter," *IEEE Trans. Instrum. Meas.*, vol. 61, no. 4, pp. 952–962, Apr. 2012.

[14] N. Zhou, D. Meng, Z. Huang, and G. Welch, "Dynamic State estimation of a synchronous machine using PMU data: A comparative study," *IEEE Trans. Smart Grid*, vol. 6, no. 1, pp. 450–460, Jan. 2015.

[15] V. M. Moreno, M. Liserre, A. Pigazo, and A. D. Aquila, "A comparative analysis of real-time algorithms for power signal decomposition in multiple synchronous reference frames," *IEEE Trans. Power Electron.*, vol. 22, no. 4, pp. 1280–1289, Jul. 2007.

[16] A. K. Singh and B. C. Pal, "Rate of change of frequency estimation for power systems using interpolated DFT and kalman filter," *IEEE Trans. Power Syst.*, vol. 34, no. 4, pp. 2509–2517, Jul. 2019.

[17] R. Chudamani, K. Vasudevan, and C. S. Ramalingam, "Real-time estimation of power system frequency using nonlinear least squares," *IEEE Trans. Power Del.*, vol. 24, no. 3, pp. 1021–1028, Jul. 2009.

[18] D. Belega, D. Fontanelli, and D. Petri, "Dynamic phasor and frequency measurements by an improved Taylor weighted least squares algorithm," *IEEE Trans. Instrum. Meas.*, vol. 64, no. 8, pp. 2165–2178, Aug. 2015.

[19] F. Messina, P. Marchi, L. R. Vega, C. Galarza, and H. Laiz, "A novel modular positive-sequence synchrophasor estimation algorithm for PMUs," *IEEE Trans. Instrum. Meas.*, vol. 66, no. 6, pp. 1164–1175, Jun. 2017.

[20] J. A. de la O Serna, "Synchrophasor measurement with polynomial phase- locked-loop Taylor–fourier filters," *IEEE Trans. Instrum. Meas.*, vol. 64, no. 2, pp. 328–337, Feb. 2015.

[21] S. Golestan, J. M. Guerrero, and J. C. Vasquez, "Single-phase PLLs: A review of recent advances," *IEEE Trans. Power Electron.*, vol. 32, no. 12, pp. 9013–9030, Dec. 2017.

[22] M. Karimi-Ghartemani, S. A. Khajehoddin, P. K. Jain, A. Bakhshai, and M. Mojiri, "Addressing DC component in PLL and notch filter algorithms," *IEEE Trans. Power Electron.*, vol. 27, no. 1, pp. 78–86, Jan. 2012.

[23] F. Wu, D. Sun, L. Zhang, and J. Duan, "Influence of plugging DC offset estimation integrator in single-phase ePLL and alternative scheme to eliminate effect of input DC offset and harmonics," *IEEE Trans Ind. Electron.*, vol. 62, no. 8, pp. 4823–4831, Aug. 2015.

[24] G. Fedele and A. Ferrise, "A frequency-locked-loop filter for biased multi-sinusoidal estimation," *IEEE Trans Signal Process.*, vol. 62, no. 5, pp. 1125–1134, Mar. 2014.

[25] G. Pin, B. Chen, and T. Parisini, "Robust finite-time estimation of biased sinusoidal signals: A Volterra operators approach," *Automatica*, vol. 77, pp. 120–132, 2017.

[26] I. Carugati, P. Donato, S. Maestri, D. Carrica, and M. Benedetti, "Frequency adaptive PLL for polluted single-phase grids," *IEEE Trans. Power Electron.*, vol. 27, no. 5, pp. 2396–2404, May 2012.

[27] G. Pin, "A direct approach for the frequency-adaptive feedforward cancellation of harmonic disturbances," *IEEE Trans. Signal Process.*, vol. 58, no. 7, pp. 3523–3530, Jul. 2010.

[28] G. Pin, B. Chen, G. Fedele, and T. Parisini, "Robust frequency-adaptive quadrature phase-locked-loops with Lyapunov-certified global stability," *IEEE Trans. Control Syst. Technol.*, vol. 31, no. 1, pp. 467–474, Jan. 2023.

[29] P. Li, F. Boem, G. Pin, and T. Parisini, "Kernel-based simultaneous parameter-state estimation for continuous-time systems," *IEEE Trans. Autom. Control*, vol. 65, no. 7, pp. 3053–3059, Jul. 2020.

[30] L. Asiminoael, F. Blaabjerg, and S. Hansen, "Detection is key-harmonic detection methods for active power filter applications," *IEEE Ind. Appl. Mag.*, vol. 13, no. 4, pp. 22–33, Jul./Aug. 2007.

[31] H. S. Lam, P. Li, B. Chen, W. M. Ng, T. Parisini, and S. Y. R. Hui, "Exponential modulation integral observer for online detection of the fundamental and harmonics in grid-connected power electronics equipment," *IEEE Trans. Control Syst. Technol.*, vol. 30, no. 5, pp. 1821–1833, Sep. 2022.

[32] H. S. Lam, H. Yuan, S.-C. Tan, C. C. Mi, J. Pou, and S. Y. R. Hui, "Bidirectional AC–DC modular multilevel converter with electric spring functions for stabilizing renewable AC power grid at the distribution voltage level," *IEEE J. Emerg. Sel. Topics Power Electron.*, vol. 10, no. 6, pp. 7589–7600, Dec. 2022.

[33] H. S. Lam, H. Yuan, N. Beniwal, J. Pou, and S. Y. Ron Hui, "An enhanced voltage control method for multilevel-converter-based electric spring at the distribution voltage level," in *Proc. 2023 IEEE Appl. Power Electron. Conf. Expo.*, 2023, pp. 966–970.
[34] H. S. Lam et al., "Modeling and practical evaluation of AC–DC solid-State transformer with electric spring functions," *IEEE Trans. Smart Grid*, vol. 15, no. 3, pp. 2831–2842, May 2024.
[35] A. Kaneko, Y. Hayashi, T. Anegawa, H. Hokazono, and Y. Kuwashita, "Evaluation of an optimal radial-loop configuration for a distribution network with PV systems to minimize power loss," *IEEE Access*, vol. 8, pp. 220408–220421, 2020.
[36] M. Li et al., "HW-DFT-based measurement method of frequency-coupling characteristics considering fundamental frequency deviation for stability analysis," *IEEE Trans. Power Electron.*, vol. 38, no. 5, pp. 6613–6626, May 2023.
[37] J. Zhang, J. Song, C. Li, X. Xu, and H. Wen, "Novel frequency estimator for distorted power system signals using two-point iterative windowed DFT," *IEEE Trans. Ind. Electron.*, vol. 71, no. 10, pp. 13372–13383, Oct. 2024.
[38] J. Borkowski, J. Mroczka, A. Matusiak, and D. Kania, "Frequency estimation in interpolated discrete fourier transform with generalized maximum sidelobe decay windows for the control of power," *IEEE Trans. Ind. Informat.*, vol. 17, no. 3, pp. 1614–1624, Mar. 2021.
[39] J. Zhao, "Dynamic State estimation with model uncertainties using H∞ extended Kalman filter," *IEEE Trans. Power Syst.*, vol. 33, no. 1, pp. 1099–1100, Jan. 2018.
[40] D. K. Gupta and R. K. Pandey, "Grid stabilization with PMU signals — A survey," in *Proc. 2014 Eighteenth Nat. Power Syst. Conf.*, 2014, pp. 1–6.
[41] J. Khodaparast, O. B. Fosso, and M. Molinas, "Recursive multi-channel prony for PMU," *IEEE Trans. Power Del.*, vol. 39, no. 2, pp. 693–705, Apr. 2024.
[42] J. G. Calderón-Guizar, M. Ramirez-González, and R. Castellanos-Bustamante, "Identification and monitoring inter-area oscillations in power systems," in *Proc. 2015 IEEE Eindhoven PowerTech.*, 2015, pp. 1–6.
[43] D. Bian, Z. Yu, D. Shi, R. Diao, and Z. Wang, "A robust real-time low-frequency oscillation detection and analysis (LFODA) system with innovative ensemble filtering," *CSEE J. Power Energy Syst.*, vol. 6, no. 1, pp. 174–183, 2020.

PENG LI (Member, IEEE) received the B.Eng. degree in control technology and instruments from North-Eastern University, Shenyang, China, in 2013, and the M.Sc. and Ph.D. degrees in control engineering from the Department of Electrical and Electronic Engineering, Imperial College London, London, U.K., in 2014 and 2019, respectively. She is currently an Associate Professor with the Harbin Institute of Technology, Shenzhen, China. Her research interests include distributed state estimation and control, identification and cooperative control of power-electronic-dominant microgrids, energy-aware autonomous perception and navigation in robotics.

HIN SANG LAM (Member, IEEE) received the B.Eng. (with First Class Hons.) degree in electrical engineering and the M.Phil. degree in electrical and electronic engineering from the University of Hong Kong, Hong Kong, in 2018 and 2020, respectively, and the Ph.D. degree in electrical and electronic engineering from Nanyang Technological University, Singapore, in 2024.

He is currently a Scientific Officer with the Department of Industrial and Systems Engineering, The Hong Kong Polytechnic University, Hong Kong. His research interests include multilevel converters, smart grids, and indoor localization.

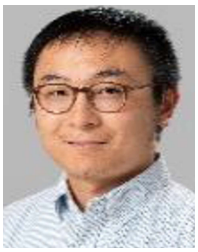

BOLI CHEN (Senior Member, IEEE) received the B.Eng. degree in electrical and electronic engineering from Northumbria University, Newcastle upon Tyne, U.K., in 2010, and the M.Sc. and Ph.D. degrees in control systems from Imperial College London, London, U.K., in 2011 and 2015, respectively. He is currently a Lecturer with the Department of Electronic and Electrical Engineering, University College London, London, U.K. His research focuses on the control, optimization, and estimation of complex dynamical systems, with rich applications in smart cities, such as, transportation, electric energy systems, and sensor networks. Dr. Boli Chen is a Member of the IEEE Control Systems Society Technical Committee on "Smart Cities". He is an Associate Editor for IEEE TRANSACTIONS ON INTELLIGENT TRANSPORTATION SYSTEMS and the *European Journal of Control*. He is a Member of the EUCA Conference Editorial Board and the IEEE ITSC Editorial Board.

RAYMOND WAI M. NG (Member, IEEE) received the B.Eng. and M.Phil. degrees in electronic engineering from the City University of Hong Kong, Hong Kong, in 1998 and 2004, respectively, and the Ph.D. degree in electrical and electronic engineering from the University of Hong Kong, Hong Kong, in 2015. From 1998 to 2000, he was an Electronic Engineer with Astec Custom Limited, Application Engineer with Ericsson Limited from 2000 to 2003. In 2009, he joined the City University of Hong Kong, as a Research Fellow. Between 2011 and 2020, he was a Research Officer and a Laboratory Manager with Smart Grid Research Facility with the University of Hong Kong. Between 2020 and 2023, he was an Assistant Technical Manager with the Department of Electrical and Electronic Engineering, University of Hong Kong. Since 2023, he has been a Senior Scientific Officer with the Department of Electrical and Electronic Engineering, Hong Kong Polytechnic University, Hong Kong. He is also a Chartered Engineer with U.K. Royal Engineering Council London, U.K., and the Institution of Engineering and Technology.

He has authored or coauthored more than twenty journal and conference papers. He is the Co-Inventor of two U.S. patents. His current research interests include power system, smart grid, and wireless power transfer.

THOMAS PARISINI (Fellow, IEEE) received the Ph.D. degree in electronic engineering and computer science from the University of Genoa, Genoa, Italy, in 1993. He was with Politecnico di Milano, Milan, Italy. Since 2001, he has been the Danieli Endowed Chair of automation engineering with the University of Trieste, Trieste, Italy. From 2009 to 2012, he was the Deputy Rector of the University of Trieste. Since 2010, he has been the Chair of industrial control. He is currently the Director of research with Imperial College London, London, U.K. He is also the Deputy Director of the KIOS Research and Innovation Centre of Excellence, University of Cyprus, Nicosia, Cyprus. He has authored or coauthored more than 280 research papers in archival journals, book chapters, and international conference proceedings. His research interests include neural-network approximations for optimal control problems, fault diagnosis for nonlinear and distributed systems, nonlinear model predictive control systems and nonlinear estimation. He was the co-recipient of the IFAC Best Application Paper Prize of the Journal of Process Control, Elsevier, for the three-year period from 2011 to 2013 and 2004 Outstanding Paper Award of IEEE TRANSACTIONS ON NEURAL NETWORKS. He was also the recipient of the 2007 IEEE Distinguished Member Award. In 2016, he was awarded as Principal Investigator at Imperial of the H2020 European Union Flagship Teaming Project KIOS Research and Innovation Centre of Excellence led by University of Cyprus. In 2012, he was awarded an ABB Research Grant dealing with energy-autonomous sensor networks for self-monitoring industrial environments. Thomas Parisini is the Vice-President for Publications Activities of the IEEE Control Systems Society and from 2009 to 2016, he was the Editor-in-Chief of IEEE TRANSACTIONS ON CONTROL SYSTEMS TECHNOLOGY. Since 2017, he has been an Editor of Control Applications of Automatica.

He the Chair of the IFAC Technical Committee on Fault Detection, Supervision & Safety of Technical Processes - SAFEPROCESS. He was the Chair of the IEEE Control Systems Society Conference Editorial Board and a Distinguished Lecturer of the IEEE Control Systems Society. He was an Elected Member of the Board of Governors of the IEEE Control Systems Society and of the European Control Association (EUCA), and a Member of the Board of Evaluators of the 7th Framework ICT Research Program of the European Union. He is an Associate Editor for the *International Journal of Control* and was an Associate Editor for IEEE TRANSACTIONS ON AUTOMATIC CONTROL, IEEE TRANSACTIONS ON NEURAL NETWORKS, *Automatica*, and *International Journal of Robust and Nonlinear Control*. He was the Program Chair of the 2008 IEEE Conference on Decision and Control and the General Co-Chair of the 2013 IEEE Conference on Decision and Control. He is a Fellow of the IFAC.

S. Y. (RON) HUI (Fellow, IEEE) received the B.Sc. (Eng) Hons. degree in electrical and electronic engineering with the University of Birmingham, Birmingham, U.K., in 1984, and the D.I.C. and Ph.D. degrees in electrical engineering with Imperial College London, London, U.K., in 1987.

He was with the University of Nottingham and University of Sydney, and an Endowed Professor with the University of Hong Kong. He is currently a Chair Professor of power electronics with the City University of Hong Kong, Hong Kong, and Imperial College London. He has authored or coauthored more than 500 research papers including 330 refereed journal publications. His IEEE Xplore patent citations exceed 1280.

More than 150 of his patents have been adopted by industry worldwide. His research interests include power electronics, wireless power, sustainable lighting, and smart grid. His inventions on wireless charging platform technology underpin key dimensions of Qi, the world's first wireless power standard, with freedom of positioning and localized charging features for wireless charging of consumer electronics. He also developed the Photo-Electro-Thermal Theory for LED Systems and Electric Spring Technology for Smart Grid. He was the recipient of the IEEE Rudolf Chope R&D Award and the IET Achievement Medal (The Crompton Medal) in 2010, IEEE William E. Newell Power Electronics Award in 2015 and the IET JJ Thomson Medal in 2024. He is a Fellow of the Australian Academy of Technology & Engineering, US National Academy of Inventors, and Royal Academy of Engineering, U.K.